Explosion of atomic clusters heated by high-intensity femtosecond laser pulses

T. Ditmire, E. Springate, J. W. G. Tisch, Y. L. Shao, M. B. Mason, N. Hay, J. P. Marangos, and M. H. R. Hutchinson
Blackett Laboratory, Imperial College of Science, Technology, and Medicine, Prince Consort Road, London SW7 2BZ, United Kingdom
(Received 5 May 1997; revised manuscript received 21 July 1997)

We have experimentally and theoretically studied the high-intensity ($>10^{16}$ W cm^{-2}), femtosecond photoionization of inertially confined noble-gas clusters. We have examined the energies of electrons and ions ejected during these interactions and found that particles with substantial kinetic energy are generated. Electrons with energies up to 3 keV and ions with energies of up to 1 MeV have been observed. These experimental observations are well explained by a theoretical model of the cluster as a small plasma sphere that explodes following rapid electron collisional heating by the intense laser pulse. [S1050-2947(97)02912-0]

PACS number(s): 36.40.−c, 52.40.Nk, 36.40.Gk

I. INTRODUCTION

Atomic clusters have long been studied by chemists and physicists because of the unique position that clusters hold as an intermediate state between molecules and solids [1]. Many studies have traced the properties of materials from their monatomic characteristics to their bulk state characteristics through an examination of the material as it forms larger and larger clusters. Experiments on the optical properties of clusters compose a sizable fraction of these studies. Photofragmentation studies in particular have been very useful in illuminating the chemistry of these atomic and molecular clusters. Many experiments involving single photon and multiphoton ionization of clusters with long laser pulses (~nanoseconds) at low to moderate intensities have been performed [2–4], and the photofragmentation [5,6] and Coulomb fission [7,8] dynamics have been extensively investigated. These experiments have revealed a number of rather interesting features about the nature of light interactions with clusters. For example, it is now well known that the absorption spectra of metallic clusters are dominated by a giant resonance due to photon coupling to a collective oscillation of the cluster electrons [9,10]. Such collective phenomena, while virtually absent in light-atom interactions, are very important in the interaction of light with clusters and can lead to remarkable optical properties.

Recently, there has been much activity in extending these studies to very high intensity, ultrashort laser pulses with peak laser intensities $>10^{15}$ W cm^{-2}, and pulse widths of 0.1–10 ps [11–22]. There has also been some preliminary theoretical work in this area [16,23]. In this parameter regime the physics governing the laser cluster interaction is fundamentally different than in previous studies. At these intensities the laser interaction is nonperturbative and very high-order multiphoton ionization and strong electric field tunnel ionization are possible. Consequently, highly charged ions can be produced [12,15,18,21]. Furthermore, the short pulses used are comparable to or shorter than the disassembly times of a cluster in the laser field [16], the entire laser pulse interacts with an inertially confined body of atoms.

Such high-intensity processes have been extensively studied in atoms and molecules. The high-intensity laser interactions with atoms have been directed toward understanding multiphoton and tunnel ionization of atoms and ions to high charge states [24,25]. Numerous studies of electron energies produced by above-threshold ionization (ATI) have also been conducted [26–28]. These studies indicate that the efficiency with which laser energy is coupled to the electrons is very low. For example, average energies of electrons produced by ATI of atoms ionized by pulses with intensity up to 10^{16} W cm^{-2} are of the order of 100 eV or less [26,28]. Many studies of the strong field laser ionization of small molecules have also been conducted in recent years [29]. These experiments have shown that the ionization mechanisms of molecules are very similar to those of single atoms. This rapid ionization by a short laser pulse subsequently results in a Coulomb explosion of the constituent ions. Ion fragments with kinetic energy of up to 100 eV have been observed in the explosion of triatomic molecules [30].

The plasmas produced by the intense illumination of solids at these high intensities have also been investigated. Unlike single atoms, intense laser interactions with high density plasmas can be very energetic. These plasmas efficiently absorb laser light due to rapid inverse bremsstrahlung heating of the plasma electrons [31]. Such plasmas can typically exhibit average electron temperatures of up to 1 keV, though they are usually clamped to lower values because of conductive cooling of the plasma [31,32]. The expansion of hot, laser-heated plasmas is usually followed by a hydrodynamic expansion into vacuum, resulting in the ejection of fast ions [33,34].

The dramatic difference between the nature of intense laser interactions with atoms and solid density plasmas points to an interesting question: do clusters of a few hundred to a few thousand atoms, objects that are small compared to a laser wavelength, behave like small molecules in strong fields or more like the energetic plasmas produced from solids? Recently a number of studies have addressed the issue of the nature of intense laser interactions with clusters over a variety of cluster sizes and laser wavelengths. These studies have ranged from ultraviolet and infrared light interactions with C_{60} molecules [35,36] to studies of interactions of clusters of more than ~100 atoms with lasers of wavelength between the ultraviolet to the near infrared [12,18]. Initial studies indicated that the intense laser interaction with clusters was much more energetic then interactions at similar intensities with atoms or small molecules. These initial stud-

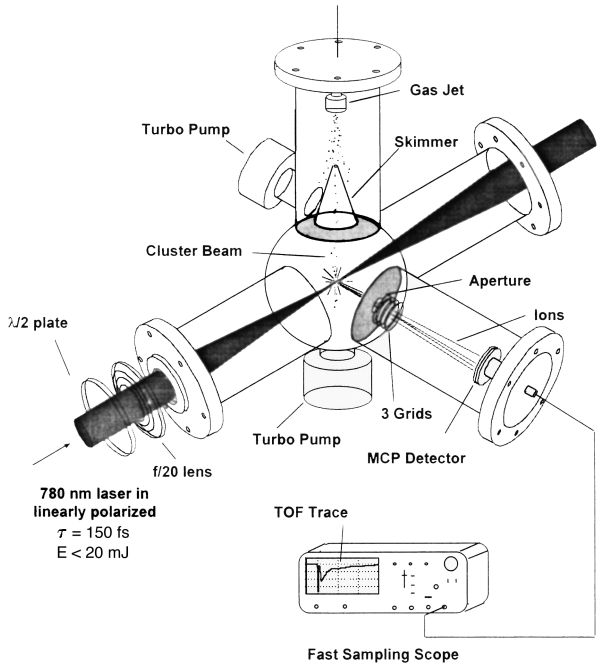

FIG. 1. Experimental configuration for measuring ion energies of exploding clusters.

ies found that intense irradiation of a medium of clusters resulted in very intense x-ray emission. In fact, x rays with energy out to 5 keV were observed in a Xe cluster gas jet irradiated by 248-nm pulses at intensity $>10^{18}$ W cm^{-2} [12]. Similar high x-ray yields have been observed in cluster media of various species and at a range of laser wavelengths [15]. These studies indirectly indicated that the clusters were absorbing substantial fractions of laser energy and were producing hot electrons and highly charged ions capable of producing the observed radiation. However, until recently, no direct data existed on the energies and distributions of either the electrons or ions ejected during the interaction of intense laser pulses with large (>1000 atom) clusters.

In this paper we present a comprehensive investigation of the physics of intense short pulse interactions with noble-gas clusters over a range of cluster sizes, species, and laser wavelengths. Direct measurements of the electron and ion energies resulting from the interactions of laser pulses with isolated clusters have been obtained. Both electrons and ions are ejected from the heated cluster with substantial kinetic energy. We find that electrons with energies up to 3 keV and ions with energies of up to 1 MeV are produced. These experimental observations are well explained by a theoretical model of the cluster as a small plasma sphere that explodes following rapid electron collisional heating by the intense laser pulse.

II. EXPERIMENTAL DETAILS

In our experiment (illustrated in Fig. 1) a beam of atomic clusters, produced in the expansion of a high-pressure gas into vacuum, is irradiated by a focused, high-intensity, femtosecond laser beam. The electrons and ions expelled from the clusters with velocities perpendicular to both the cluster beam and the laser beam propagate along a flight tube and are detected by a microchannel plate detector (MCP). The ion energies are then determined by time-of-flight measurements; the electron energies are found by measuring the decrease in the MCP signal as a retarding voltage is applied to a grid placed between the focus and the MCP.

The laser used was a high-power Ti:sapphire laser, based on the principle of chirped pulse amplification, which delivers 150-fs pulses at a wavelength of 780 nm. This laser has been discussed at length in Ref. [37]. In brief, near-transform-limited 90-fs pulses are produced by a Kerr lens mode-locked Ti:sapphire oscillator. These pulses are stretched to 250 ps with a grating stretcher and are then amplified in a Ti:sapphire regenerative amplifier followed by a Ti:sapphire multipass power amplifier to an energy of ~ 80 mJ. After recompression, the final pulse duration is 150 fs, the $1/e^2$ diameter of the beam is 1.5 cm$\times 2$ cm and the maximum pulse energy is 40 mJ.

The laser is focused using a plano-convex lens with a focal length of 20 cm. With this focal configuration the focal spot size is found to be nearly Gaussian with a $1/e^2$ diameter of $\sim 40\ \mu$m, which is ≈ 4 times diffraction limited. This yields a peak focused intensity of $\sim 2\times 10^{16}$ W cm^{-2} with 20 mJ of laser intensity. This intensity was confirmed in a separate experiment by observing the appearance of He^{2+} through tunnel ionization, which occurs at an intensity of $\sim 7\times 10^{15}$ W cm^{-2} [25].

A solenoid pulsed gas jet valve produced the noble-gas clusters in our experiment. The extent of atomic clustering in our gas jet can be estimated using Hagena's empirical scaling parameter [38,39],

$$\Gamma^* = k\,\frac{(d/\tan\alpha)^{0.85} p_0}{T_0^{2.29}}, \tag{1}$$

which assumes that the extent of clustering is dependent only on d the diameter of the nozzle (in μm), α the jet expansion half-angle, p_0 the gas-jet backing pressure in mbar, T_0 the initial gas temperature, and k the condensation parameter. The condensation parameter is an empirical constant that depends on the gas ($k=5500$ for Xe, 2900 for Kr, and 4 for He [39]). In our experiment, $d=500\ \mu$m, $\alpha=45°$, and $T_0=298$ K, so, with a backing pressure of 6 bar, Γ^* is 14 000 for xenon, 7400 for krypton, and 10 for helium. Published scalings of cluster size with the Hagena parameter indicate that the onset of massive condensation in the gas jet (where the majority of atoms condense into clusters of >100 atoms) occurs at $\Gamma^* \sim 1000$ [39].

To establish the presence of clusters in our gas jet and determine their average size we conducted a series of Rayleigh scattering measurements. Low-power, vertically polarized 532-nm light from a frequency-doubled Nd:YAG laser (100 μJ in a 10-ns pulse) was focused by an $f/30$ lens to 3 mm below the gas-jet nozzle. An $f/4$ lens imaged the 90° side-scattered light from this region through a small aperture, and it was detected by a photomultiplier fitted with a narrow-band, 532-nm interference filter. The scattered signal as a function of backing pressure, p_0, for xenon, krypton, and helium is shown in Fig. 2.

Our measurements indicate that clusters of a detectable size begin to form at pressures around 1000 mbar in xenon

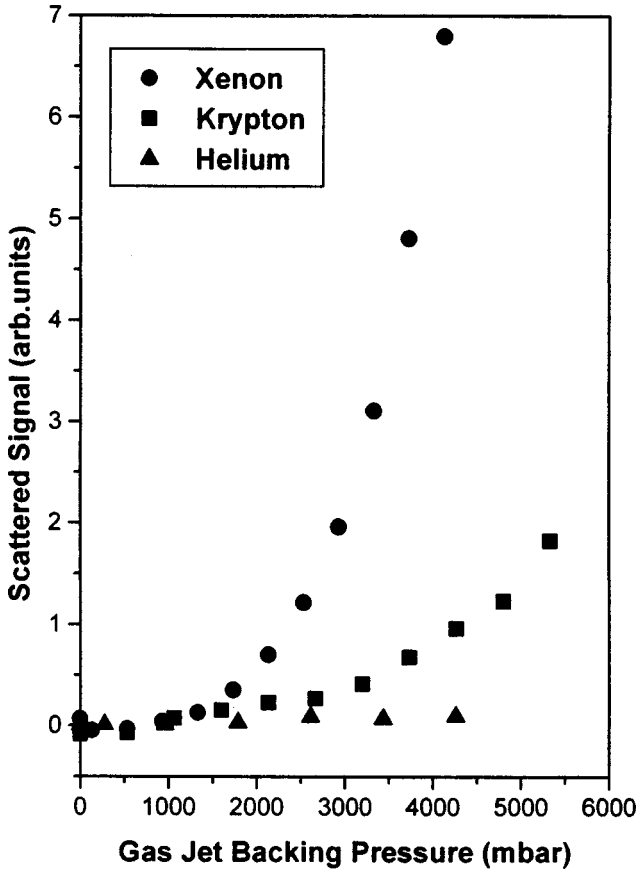

FIG. 2. Measured Rayleigh scattered light signal as a function of gas-jet backing pressure for xenon, krypton, and helium.

and 2000 mbar in krypton. In helium, which has a condensation parameter three orders of magnitude smaller than those of xenon and krypton and is not expected to cluster under these conditions, no scattered signal above the noise level was observed. The scattered signal from the Xe and Kr clusters displays a p_0^3 dependence with increasing backing pressure. This is consistent with a simple scaling argument. The scattered signal S_{RS} is proportional to the product of the Rayleigh scattering cross section of the cluster and the density of clusters, n_c. At a given wavelength, the cross section scales as R_c^6, where R_c is the radius of the cluster, so

$$S_{\mathrm{RS}} \sim n_c R_c^6. \tag{2}$$

If we assume that all the atoms have condensed into clusters, it then follows that the number density of clusters will be given by the monomer density before clustering, n_0, divided by the number of atoms per cluster, N_c, so

$$n_c \sim n_0 / N_c, \tag{3}$$

Substituting Eq. (3) into Eq. (2) and using the fact that $R_c \sim (N_c)^{1/3}$ we obtain

$$S_{\mathrm{RS}} \sim n_0 N_c. \tag{4}$$

The monomer density before clustering is known to be proportional to the backing pressure p_0 so we have

$$S_{\mathrm{RS}} \sim p_0 N_c. \tag{5}$$

TABLE I. Calibration of xenon and krypton cluster size with gas-jet backing pressure. Error in estimate of number of atoms per cluster ~ factor of 2.

	Xenon		Krypton	
Pressure (bar)	Number of atoms, N_c	Cluster radius, R_c (Å)	Number of atoms, N_c	Cluster radius, R_c (Å)
1	100	11	30	7
2	400	18	120	11
3	900	24	270	14
4	1600	29	480	17
5	2500	33	750	20
6	3600	37	1080	23

Our observation that the scattered signal varies as $\sim p_0^3$ is consistent with published scalings of cluster size with gas-jet backing pressure, which show a quadratic dependence of cluster size N_c on backing pressure p_0 [39].

The average cluster size at a particular backing pressure (Table I) was estimated from the Rayleigh scattering data of Fig. 2. We have assumed that the observed onset of clustering corresponds to roughly 100 atoms per cluster and we then use the measured increase in scattered signal to calculate the cluster size as a function of backing pressure. Using this scaling we can infer that, at $p_0 = 4$ bar, an average xenon cluster will contain ~ 1600 atoms and have a radius $R_c \approx 29 \pm 7$ Å, while a krypton cluster will typically contain ~ 500 atoms and have a radius $R_c \approx 17 \pm 4$ Å. Our scattering technique only yields information on the average size of the clusters; it does not give us any information on the size distribution of the clusters.

The clusters produced by the gas jet were collimated into a low-density cluster beam for the time-of-flight experiments. A skimmer with an aperture of 0.5 mm and 50° cone located 20 cm below the gas jet was used to collimate the cluster beam and separate the chamber containing the gas jet from the interaction region and TOF spectrometer. This produced a low-density cluster beam that intercepted the laser beam at the focus. The two chambers were differentially pumped to enable cluster formation in the gas jet while ensuring that the vacuum in the interaction region remained sufficiently low. The base pressure in the main chamber was $\sim 10^{-7}$ mbar. The gas jet was run on a 1-Hz cycle with an opening time of 400 μs, giving a maximum background pressure in the main chamber of $\sim 10^{-6}$ mbar. Electron and ion signals were only observed when the laser pulse and the arrival of clusters from the gas jet were coincident.

The electrons emitted in the interaction were detected by a two-stage microchannel plate placed at the end of a 17-cm flight tube, oriented perpendicular to both the cluster beam and the laser beam. The area subtended by the MCP detector limited the detection cone to 3.5×10^{-3} sr. Two grids (spaced 3 mm apart) were placed immediately behind the entrance to the flight tube. The first grid was charged to a voltage Φ and the second was grounded, introducing a potential barrier to electrons with energy less than $e\Phi$. The front plate of the MCP was grounded and the back held at $+2$ kV. The MCP output was capacitively coupled to a fast digital oscilloscope and fast gated integrators, which were

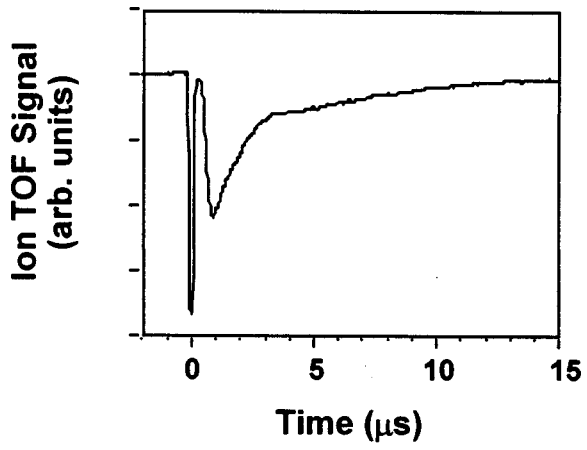

FIG. 3. Time-of-flight spectrum from 2500-atom xenon clusters (backing pressure 5 bar) irradiated by a peak intensity of 2×10^{16} W cm^{-2}. The 38-cm flight tube was field free, but electrons with energy <2 keV are not detected as the front plate of the MCP is charged to $+2$ kV.

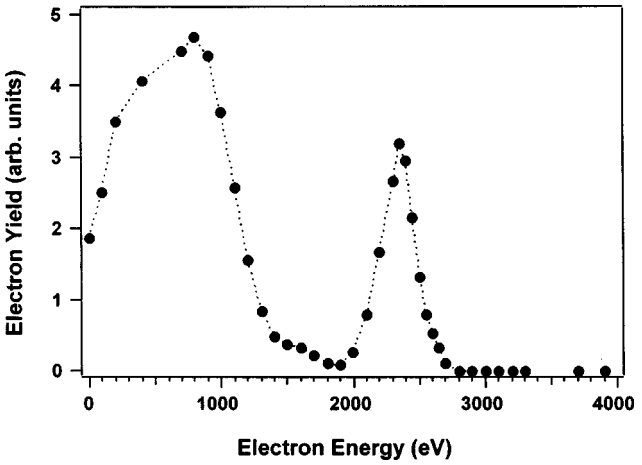

FIG. 4. Measured electron energy distribution from xenon clusters for a peak intensity of 1.5×10^{16} W cm^{-2}. The gas-jet backing pressure was 4.5 bar, corresponding to an average cluster size of 31 Å or 2100 atoms.

interfaced with a PC. The electron signal was measured as a function of retarding voltage, smoothed with a three-point adjacent averaging routine, and differentiated to give the electron energy spectrum. Each data point is the average of 50 shots, taken within a $\pm10\%$ laser energy bin.

The ion energies were determined by measuring their flight time in the field-free drift tube, which was extended to 38 or 80 cm for these measurements. The front plate of the MCP was held at -2 kV and the back plate was at earth. A grounded metal grid placed ~2 mm before the MCP ensured that the flight tube was field free. The signal was again processed by a fast digital oscilloscope (with the bandwidth limited to 20 MHz).

A typical time-of-flight spectrum (which represents the average of ~1000 laser shots) is shown in Fig. 3. The fast peak a few nanoseconds after the trigger is due to electrons with energies above 2 keV, while the broad signal extending from ~0.5 μs is due to ions. The ion time-of-flight spectrum was converted to an energy spectrum after smoothing with an eleven-point adjacent averaging routine. The TOF trace yields the ion distribution function $f(t)dt$. To retrieve the energy distribution function $f(E)dE$, the number of ions in each time bin was divided by dE/dt (which is $m_i l^2 t^{-3}$, where m_i is the ion mass, l the length of the flight tube, and t the flight time). This factor tends to shift the peak of the ion spectrum from fast flight times to lower energies.

We have not made any additional corrections to the ion energy spectrum to account for the variation in detection sensitivity with different ion energies. Because of the presence of the grounded grid immediately in front of the negatively charged microchannel plate, all ions experience some charge-state dependant acceleration prior to striking the plates. Thus ions that travel along the flight tube with a small amount of energy (say <10 keV) will acquire some substantial amount of energy in the small (2 mm) region between the grounded grid and front plate (2000 eV times the charge state of the ion). This ensures that, though there is large variation in the energy of the ions ejected from the clusters (a factor of 10^4), there is a much smaller variation in the energies of the ions striking the detector (less then a factor of ~50). This fact, coupled with the fact that the variation of the detector sensitivity with ion energy is quite low, indicates that this effect will not have a large effect on the shape of the ion energy spectrum.

Three metal grids, spaced ~3 mm apart, were placed along the flight tube roughly one-third of the distance from the laser focus. Charging the middle grid to a potential Φ while keeping the front and back grids at earth introduced a barrier to ions with energy less than $Ze\Phi$ (where Z is the charge on the ion) without significantly altering the flight time of higher energy ions. By varying the voltage we were able to measure the charge-state distribution of the ions as a function of their kinetic energy. The number of ions of a given energy, $E\pm\Delta E$ ($\Delta E=20\%$), was calculated for each value of the retarding potential, Φ. This gives the number of ions with charge Z greater than $(E\pm\Delta E)/\Phi$. This was smoothed with a three-point adjacent averaging routine and then differentiated to give the number of ions in each charge state with energy $E\pm\Delta E$.

III. EXPERIMENTAL RESULTS

A. Electron energy spectra

The measured energy spectrum of electrons emitted along the direction of the laser polarization during the irradiation of clusters of ~2100 xenon atoms (4.5 bar backing pressure) with an intensity of 1.5×10^{16} W cm^{-2} is shown in Fig. 4. There are two distinct features in the electron energy spectrum. The first, broad peak consists of what we shall call ''warm electrons'' with energies ranging from 0.1 to 1 keV. A second, sharper peak (referred to as the ''hot electrons'' throughout this paper) appears at 2.5 keV. Both peaks are only present when the laser interacts with Xe clusters. When the interaction region contains only monatomic xenon (in a static fill) we detect no electrons with energy above 100 eV.

The most remarkable aspect of this energy distribution are the high electron kinetic energies, with a large fraction of the electrons having energies between 2 and 3 keV. Previous measurements of ATI spectra from single atoms at this intensity and pulse duration have indicated that the vast major-

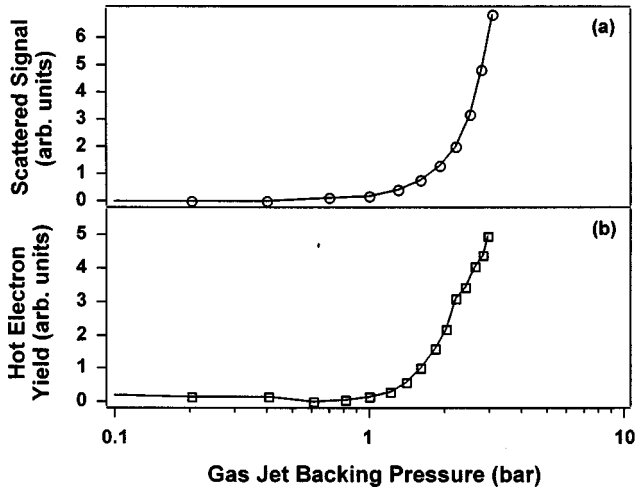

FIG. 5. (a) Measured Rayleigh scattering signal as a function of xenon backing pressure (as in Fig. 2). (b) Measured yield of hot electrons for a peak intensity of 1×10^{16} W cm^{-2} as a function of xenon backing pressure

ity of electrons produced have energies below 100 eV [26,28]. Only a very small fraction of electrons (typically 10^{-3}–10^{-4}) have higher energy, with no detectable electrons having an energy of above 1 keV [28]. The spectrum observed from Xe clusters clearly indicates a much greater coupling of laser energy to electrons than is present during the irradiation of single atoms. Furthermore, this spectrum indicates that the laser-cluster interaction produces even hotter electron temperatures than a laser-solid interaction at this intensity, where electron temperatures of 100–500 eV are typical [32].

Examining the hot electron yield as a function of gas-jet backing pressure provides more evidence that this signal results from the interaction of the laser with clusters rather than atoms. Figure 5 shows the close correlation of the onset of hot electron production with the onset of clustering in xenon. The hot electron production [Fig. 5(b)] was measured by integrating the hot electron MCP signal over time, while Fig. 5(a) (identical to Fig. 2) shows the Rayleigh scattering signal from the gas jet. Both hot electron production and clustering have a sharp onset at a gas-jet backing pressure of 1 bar. Below this backing pressure the gas jet beam with which the laser interacts is composed primarily of single Xe atoms or small (<10 atom) clusters. No hot electrons are observed in this situation. Only the production of large Xe clusters results in a measurable hot electron signal. The warm electron signal exhibits similar scaling.

The presence of two distinct peaks in the electron energy spectrum suggests that these two groups may be produced under different conditions at different times in the cluster expansion. This assumption is supported by examining the angular dependence of the electron emission with respect to the laser polarization (Fig. 6). The angle between the direction of polarization and the detector was varied with a $\lambda/2$ plate placed before the entrance to the vacuum chamber. We exploited the different flight times of the two sets of electrons to discriminate them and then integrated the MCP signal over an appropriate time gate. The measured angular distribution of warm electrons is shown in Fig. 6(a), and that of the hot electrons in Fig. 6(b).

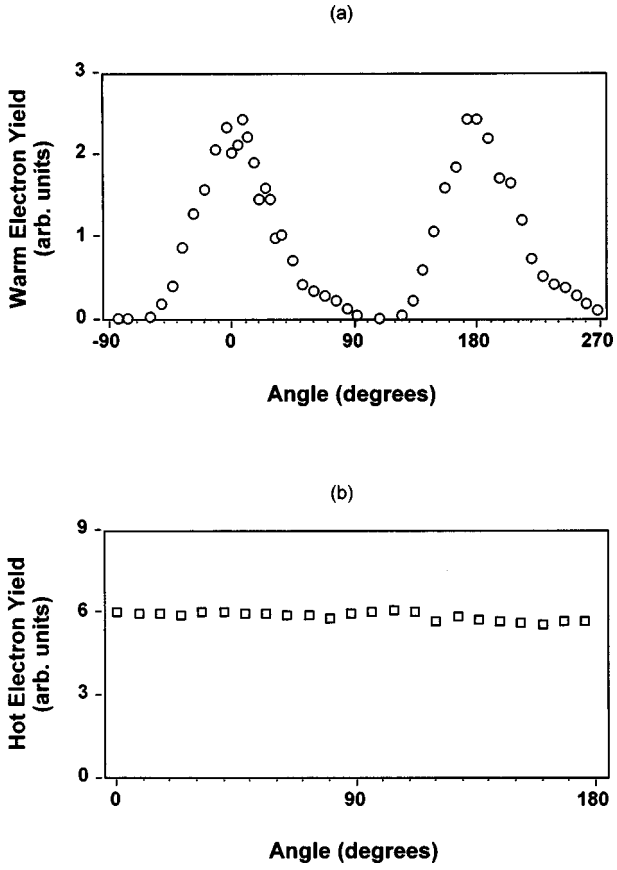

FIG. 6. (a) Angular distribution of ''warm electrons'' with energies ranging from 0.3 to 1 keV. Emission along the direction of laser electric field polarization is defined as being at 0° and 180°. (b) Angular distribution of ''hot electrons'' with energies ranging from 2 to 3 keV. The gas-jet backing pressure was 4 bar, corresponding to an average cluster size of 1600 atoms.

The angular distributions of the two groups of electrons are markedly different. The hot electron emission is completely isotropic, having no variation with respect to the direction of the laser polarization, while warm electron emission is peaked along the laser polarization. The warm electron peak has a full width at half maximum of about 60°. Both these distributions are significantly different from the angular distributions associated with single atoms. The electrons from high-order ATI are expected to have a much narrower angular distribution (a width of 15–20°, peaked along the laser polarization, was reported in Ref. [26]). In high field tunneling ionization, the narrow angular distribution stems from the much higher tunneling rate in the direction of the laser field. The electrons observed in our experiment cannot, therefore, be interpreted as simply resulting from the tunnel ionization of individual atoms. Some rescattering of the electrons by ions in the cluster is necessary to explain the broadening observed in the warm electron distribution. The isotropic distribution of the hot electrons indicates that these electrons have undergone many electron-ion collisions in the laser field, completely randomizing their velocity distribution.

B. Ion energy spectra

The remarkably high energies of the electrons produced in the intense laser-cluster interaction suggests that highly

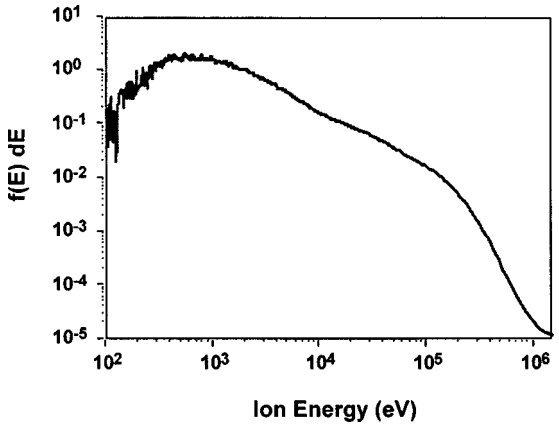

FIG. 7. Ion energy spectrum from clusters of 2500 Xe atoms (backing pressure 5 bar) irradiated by a peak intensity of 2×10^{16} W cm^{-2}, derived from the time-of-flight trace shown in Fig. 3.

charged ions with large kinetic energies may also be ejected from the cluster. Charge separation of these hot electrons will inevitably accelerate the cluster ions to high velocities. Such hot ions are, in fact, observed as the TOF trace in Fig. 3 illustrates.

The energy spectrum of ions resulting from the interaction of $\sim$2500-atom Xe clusters with a laser pulse of intensity $\sim2\times10^{16}$ W cm^{-2} is shown in Fig. 7 (obtained from the TOF trace in Fig. 3). The most remarkable aspect of this energy distribution is the presence of ions with energies up to 1 MeV. This energy is four orders of magnitude higher than has previously been observed in the Coulomb explosion of molecules [30] and about 1000 times higher than the average energy of the highest charge state Ar ions ejected in the disintegration of small clusters of up to six argon atoms irradiated at 10^{15} W cm^{-2} reported by Purnell *et al.* [14]. The average ion energy of this distribution, defined as

$$\overline{E}=\frac{\int Ef(E)dE}{\int f(E)dE}, \tag{6}$$

is 45 ± 5 keV. Thus the average laser energy deposited per ion is also substantial.

Figure 8 shows the raw time-of-flight signal from 1600-atom clusters as a function of angle with respect to the direction of laser polarization. The polarization was rotated, as before, by placing a $\lambda/2$ plate in the beam path just before the vacuum chamber. The ion energy distribution is isotropic with respect to the direction of laser polarization, apparently a consequence of a spherically exploding cluster.

Our ability to control the cluster size by changing the backing pressure of the gas jet enables us to examine the scaling of the ion energy distribution with cluster size (Fig. 9). We find that both the maximum energy $E_{\max}$ (defined as the energy at which the signal drops to 10^{-5} of its maximum) and average energy E of the ion distribution increase slowly with increasing cluster size. At a pressure of 5 bar, corresponding to 2500 atoms/cluster, $E_{\max}$ is 1 MeV and E is 41 keV, while at 2 bar (400 atoms/cluster), $E_{\max}$ is 200 keV and E is 29 keV. Though there is a slight drop in the energies of the ions produced, there is no dramatic shift in the shape

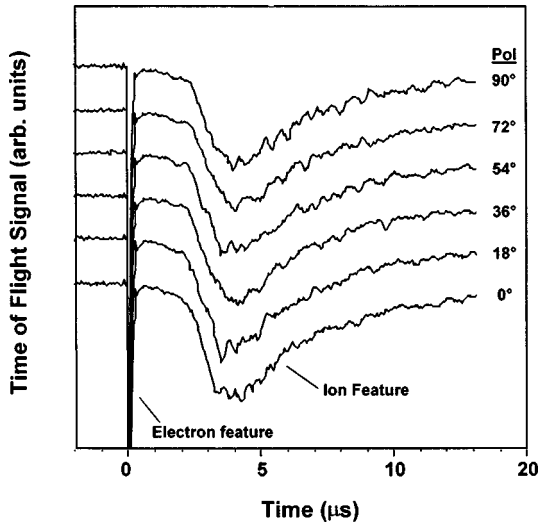

FIG. 8. Time-of-flight traces of ions produced by the irradiation of clusters of 1600 Xe atoms (backing pressure 4 bar) with a peak intensity of 1×10^{14} W cm^{-2}. Each plot is the average of 500 laser shots. Each curve (offset for clarity) has been taken with a different angle between the laser polarization and the detection axis. The direction of laser polarization is defined as being 0°. The flight tube was extended to 80 cm for these measurements.

of the ion distribution as the cluster size is increased. This suggests that the mechanism driving the cluster ion explosion does not dramatically change as the cluster size is varied from a few hundred to a few thousand atoms per cluster.

We observe no hot ions (with energies above 1 keV) at backing pressures below 1 bar. This pressure corresponds both to the onset of massive condensation in the gas jet (where the majority of atoms condense into clusters of >100 atoms), and to the onset of hot electron production from the exploding clusters. This points to a change in the dynamics of the cluster expansion once the cluster size increases to above ~100 atoms.

Similar behavior is found in the explosion of Kr clusters, though the explosions are not as energetic as those of the Xe clusters under similar conditions. The ion energy dis-

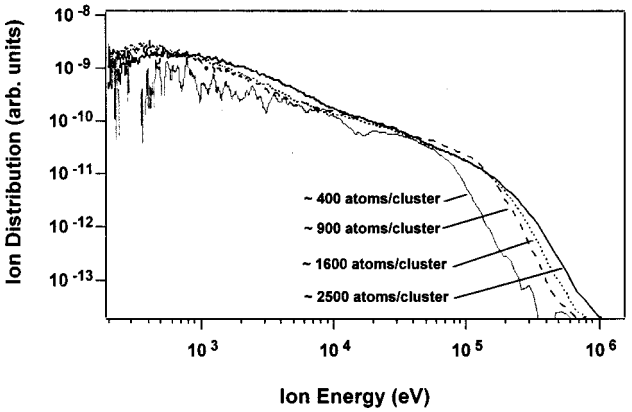

FIG. 9. Ion energy spectra from clusters of 400, 900, 1600, and 2500 xenon atoms (backing pressure 2, 3, 4, and 5 bar respectively) irradiated by a peak intensity of 2×10^{16} W cm^{-2}. The average ion energies are 29 keV for 400 atoms/cluster, 38 keV for 900 atoms/cluster, 39 keV for 1600 atoms/cluster and 41 keV for 2500 atoms/cluster.

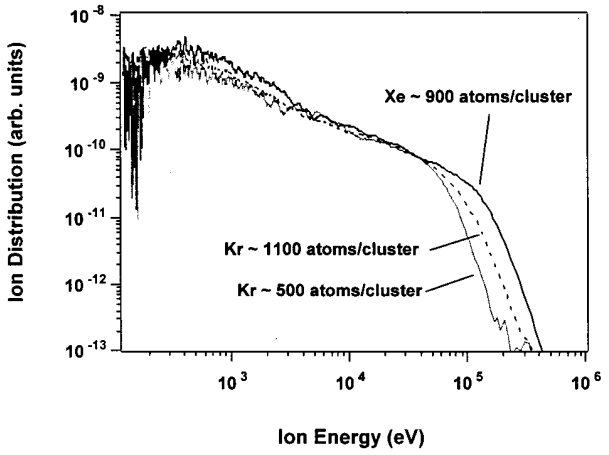

FIG. 10. Ion energy spectra from 1100-atom and 500-atom krypton clusters (backing pressures 6 and 4 bar respectively) and from 900-atom xenon clusters (backing pressure 3 bar). The average ion energies of the krypton clusters are 28 keV for 1100 atoms/cluster and 23 keV for 500 atoms/cluster, compared to 38 keV for clusters of 900 xenon atoms. The peak laser intensity was 2×10^{16} W cm^{-2}.

tribution in krypton clusters as a function of gas-jet backing pressure is shown in Fig. 10. The shape of the energy spectrum is very similar to that obtained from xenon clusters. At a pressure of 6 bar (1100 atoms/cluster), $E_{\max}$ is 350 keV and

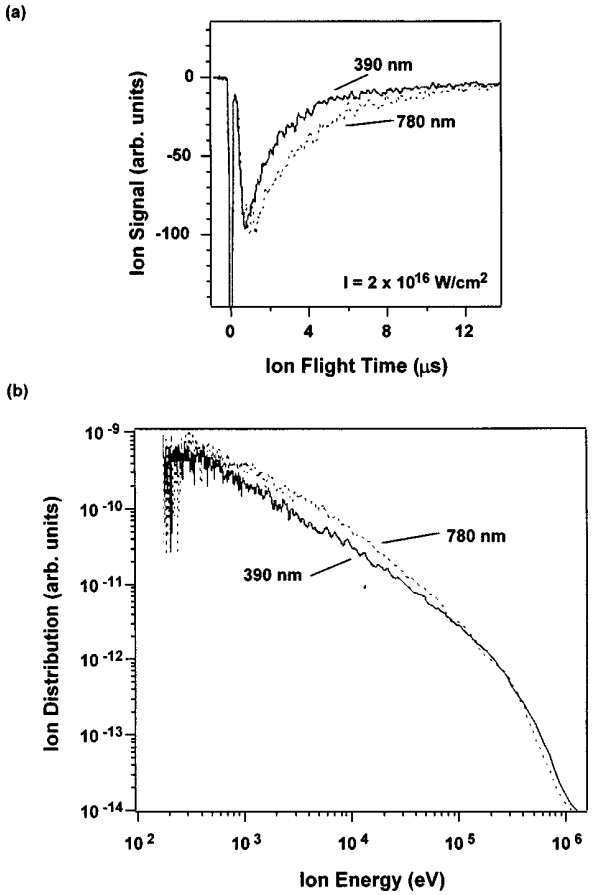

FIG. 11. Ion TOF trace with 38-cm flight tube (a) and corresponding ion energy spectrum (b) for clusters of 2500 Xe atoms irradiated with a peak intensity of 2×10^{16} W cm^{-2} at 780 nm, and at 390 nm.

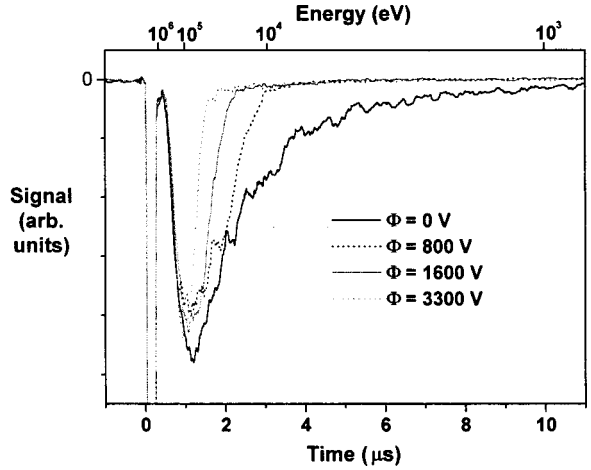

FIG. 12. Ion TOF traces with 38-cm flight tube of 2500-atom Xe clusters (backing pressure 5 bar) irradiated with a peak intensity of 2×10^{16} W cm^{-2} at retarding voltages of 0, 800, 1600, and 3300 V.

$\overline{E}$ is 28 keV, while at 4 bar (500 atoms/cluster), $E_{\max}$ is 250 keV and $\overline{E}$ is 23 keV. The average and maximum energies for a given cluster size are slightly lower in krypton than xenon.

C. Cluster explosion with ultraviolet irradiation

Though all of the data presented to this point have been taken with near infrared radiation at a wavelength of 780 nm, we have also conducted a preliminary study of the nature of the cluster ion explosion in ultraviolet light. For these experiments, the laser was frequency doubled to a wavelength of 390 nm using a 3-mm-thick potassium dihydrogen phosphate (KDP) crystal. Up to 5 mJ of light was focused into the TOF chamber with a lens of 20 cm focal length.

Figure 11 shows a comparison of the ion energies obtained when clusters of ~2500 xenon atoms were irradiated with 780- and 390-nm light at intensity of 2×10^{16} W cm^{-2} [Fig. 11(a) is the TOF trace and 11(b) is the corresponding energy spectrum]. In general we find that the shape of the ion TOF trace produced with UV light is very similar to that produced with the IR pulse. The ions from the UV irradiation appear to be slightly hotter. This can be most easily seen in the comparison of the TOF traces. The UV generated ion signal peaks in the same place as the IR signal, however, there are fewer ions at times >1 μs. Nonetheless, the differences between the UV and the IR traces are relatively small.

D. Charge-state distributions

Another striking feature of the ions produced from the cluster explosion is ionization to very high charge states—a feature that has already been seen in Refs. [12], [15], and [21]. Figure 12 shows the time-of-flight spectra from ~2500-atom xenon clusters irradiated by 2×10^{16} W cm^{-2} at kinetic energies from 1 to 100 keV as the retarding voltage Φ is varied from 0 to 3.3 kV. The retarding voltage introduces a potential barrier to ions with energies less than $Ze\Phi$, without significantly altering the flight times of higher-energy ions. The charge-state distributions calculated from

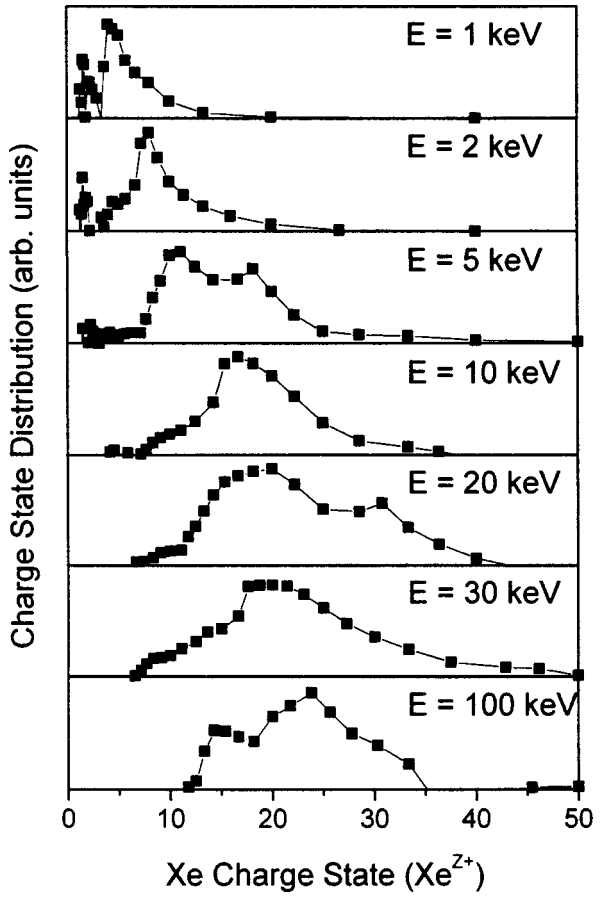

FIG. 13. Measured charge-state distribution of 2500-atom Xe clusters (backing pressure 5 bar) irradiated with a peak intensity of 2×10^{16} W cm^{-2} for ion kinetic energies of 1, 2, 5, 10, 20, 30, and 100 keV.

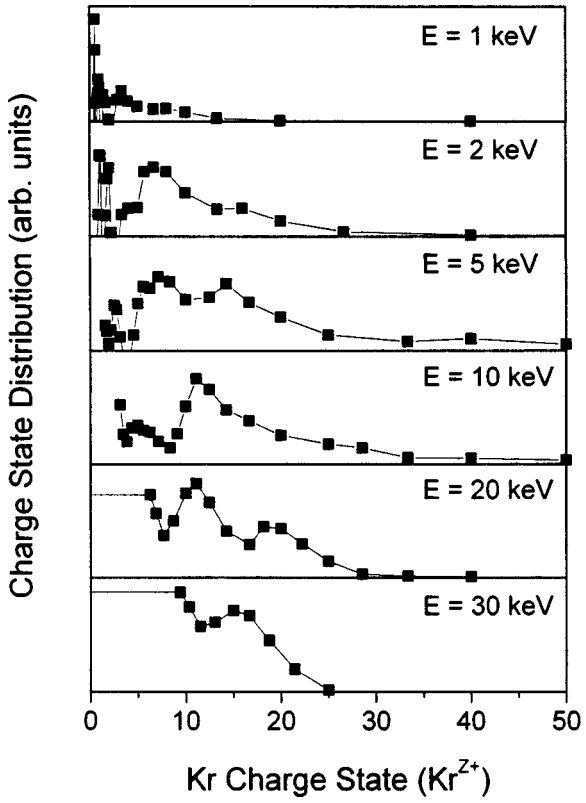

FIG. 14. Measured charge-state distribution of clusters of 1100 Kr atoms (backing pressure 6 bar) irradiated with a peak intensity of 2×10^{16} W cm^{-2} for ion kinetic energies of 1, 2, 5, 10, 20, and 30 keV.

these spectra are shown in Fig. 13, while Fig. 14 shows those from ~1100-atom krypton clusters at the same intensity.

For high energy Xe ions, the peak is at $Z=18^{+}-25^{+}$, with some ions having charge states as high as 40^{+}. The peak for high-energy krypton ions is at $12^{+}-17^{+}$ with the highest charge state present being around $Z=25^{+}$. These are much higher charge states than those expected from field ionization of single atoms at these intensities. We would expect to see charge states out to 12^{+} in xenon and 8^{+} in krypton at an intensity of 2×10^{16} W cm^{-2} [25]. Ionization to Xe^{40+} would require an intensity of nearly 10^{20} W cm^{-2} if the ionization were due to tunnel ionization alone. High-temperature electrons in the cluster, which are created through laser-driven heating, strip the ions to higher charge states by collisional ionization. The ion charge state depends only weakly on ion kinetic energy, contrary to what would be expected from a simple Coulomb explosion, and to the results reported in [14] for the Coulomb explosion of very small argon clusters.

IV. THEORETICAL AND NUMERICAL ANALYSIS

The very-high-energy particles observed experimentally are dramatically different from those typically produced in strong-field laser interactions with molecules. Such energies are typical of particles produced in the interaction of a high intensity laser with solid density plasmas. This suggests that the appropriate way to explain the exploding cluster behavior is to treat it as a small microplasma. Consequently, we have modeled the exploding clusters using the formulation first detailed by Ditmire *et al.* [16]. In this treatment the cluster is treated as a classical, spherical plasma ball of uniform density. This treatment is appropriate when the charge of the cluster is sufficient to retain electrons within the vicinity of the cluster following their ionization from the constituent atoms.

This picture of the cluster implies a number of interesting consequences. First, because of the high electron and ion densities within the cluster, electron collisional processes will be very important. In particular, the electrons will undergo rapid heating by the laser field due to electron-ion collisions (inverse bremsstrahlung). This process converts the coherent oscillation energy of the electron cloud to random thermal energy. Electron collisional ionization will also be important, stripping the constituent atoms to very high charge states.

The second consequence of viewing the cluster as a sphere of plasma is that the cluster, which becomes conducting once some electrons have been liberated by ionization, will exhibit some of the optical properties of metallic clusters. The most remarkable property of metallic clusters is the presence of a giant resonance in the optical absorption spectrum [10], which is a result of a resonantly driven oscillation of the entire cluster electron cloud. This resonance occurs when the light frequency is near to the plasma frequency of the electrons in the cluster. (The actual plasma density at the resonance is dependent upon the shape of the cluster.) The

presence of this resonance turns out to be very important in the dynamics of the high-intensity laser interaction with the cluster.

To explore the interplay of these effects we have used the numerical model for the cluster evolution first detailed in Ref. [16]. This numerical model treats the cluster as a spherical microplasma, subject to the standard processes of a laser-heated plasma. The model solves for ionization in the cluster, including rates for laser field tunnel ionization [40] and both thermal and laser-driven electron collisional ionization [41]. Laser-driven collisional heating in the cluster is found using the standard Silin formulas [42] for the electron-ion collision frequency. The model calculates the free streaming rate of electrons leaving the cluster, accounting for the mean free path of electrons in the cluster. Only electrons with energy sufficient to overcome the Coulomb attraction of the positively charged cluster are allowed to leave. The cluster expansion, assumed to be uniform and isotropic, is calculated accounting for hydrodynamic and Coulomb repulsion forces within the charged cluster. The electron energy distribution within the cluster is assumed to be Maxwellian throughout the calculation.

To account for the collective electron oscillation effects on the optical absorption of the cluster we use a zero-frequency approximation for the laser field. This approximation is appropriate when the cluster is much smaller than the laser wavelength. It also assumes that the response of the cluster electron cloud is fast compared to the time scale of the cluster expansion dynamics. Using these assumptions and the approximation of the cluster as a ball of uniform density, we can calculate the electric field inside the cluster using the formula for the electric field of a dielectric sphere in a uniform electric field [43]. The electric field in the cluster is therefore

$$E = E_0 \frac{3}{|\varepsilon + 2|}, \tag{7}$$

where E_0 is the laser electric field in vacuum. The cluster dielectric constant is given by the Drude model for a plasma,

$$\varepsilon = 1 - (n_e/n_{\mathrm{crit}})(1 + i\nu/\omega)^{-1}, \tag{8}$$

where n_e is the electron density, n_{crit} is the electron critical density for a laser field of frequency ω, and ν is the electron-ion collision frequency. This formula predicts that when $n_e/n_{\mathrm{crit}} > 6$ the electric field inside the cluster is shielded by the oscillating electron cloud and the field inside the cluster is smaller then the surrounding field in vacuum. On the other hand, Eq. (1) has a sharp maximum when $n_e/n_{\mathrm{crit}} = 3$. At this point the oscillating laser field resonantly drives the cluster electron cloud and the field inside the cluster is enhanced. As a result, the free electrons in the cluster undergo rapid collisional heating because of the local increase in the field energy density. The numerical model self-consistently treats all laser-driven processes (such as tunnel ionization and collisional heating) subject to this equation for the electric field.

An example of the dynamics of a xenon cluster are illustrated in Fig. 15. Here the calculated time history of a 30-Å Xe cluster ($\sim$1800 atoms) irradiated by a 140-fs pulse with a peak intensity of 2×10^{16} W cm^{-2} is shown. The laser pulse envelope is shown in Fig. 15(a). Figure 15(b) illustrates the radius of the cluster as a function of time; Fig. 15(c) shows the electron density (normalized to the critical density), and Fig. 15(d) shows the electron temperature.

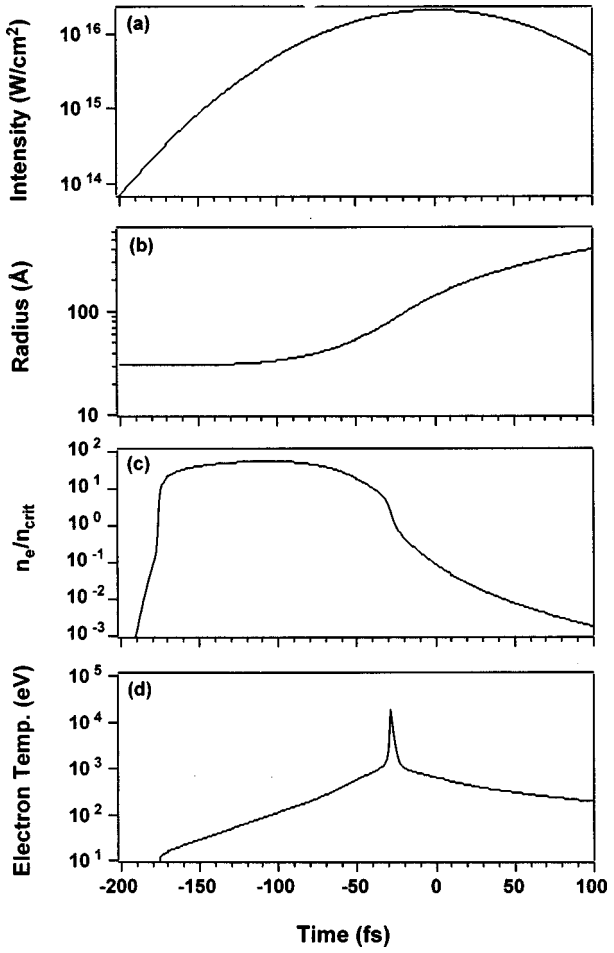

FIG. 15. Theoretical calculations of the time history of 30-Å Xe clusters (1800 atoms/cluster) irradiated by a 140-fs pulse with a peak intensity of 2×10^{16} W cm^{-2}. (a) Laser pulse envelope, (b) cluster radius, (c) electron density, n_e (normalized to the critical density, n_{crit}), and (d) electron temperature.

Early in the laser pulse, around $t \approx -190$ fs, optical ionization creates some free electrons in the cluster. Though a few of the initially ionized electrons escape from the initially neutral cluster, the space charge of the cluster keeps additional electrons from escaping. These electrons will then start to acquire thermal energy from the laser field through Coulomb collisions with the ions in the cluster. The temperature of the electrons begins to rise at $t \approx -175$ fs. In addition, the free electrons in the cluster will begin to collisionally ionize the Xe ions in the cluster. The cluster begins to expand and the electron heating continues. The heating of the electrons in the initial phase of the interaction is low due to the shielding of the laser field by the high free electron density that has been created in the cluster. Ultimately, at $t \approx -30$ fs, the expansion of the cluster lowers the electron density to bring the electron oscillation into resonance with the laser field. This results in a very rapid deposition of the energy into the electrons, causing the sharp spike in the electron temperature seen in Fig. 15(d). At this point, the ions are very rapidly stripped by the hot electrons. The cluster then explodes, manifested by the rapid expansion seen in Fig. 15(b) following the resonant heating.

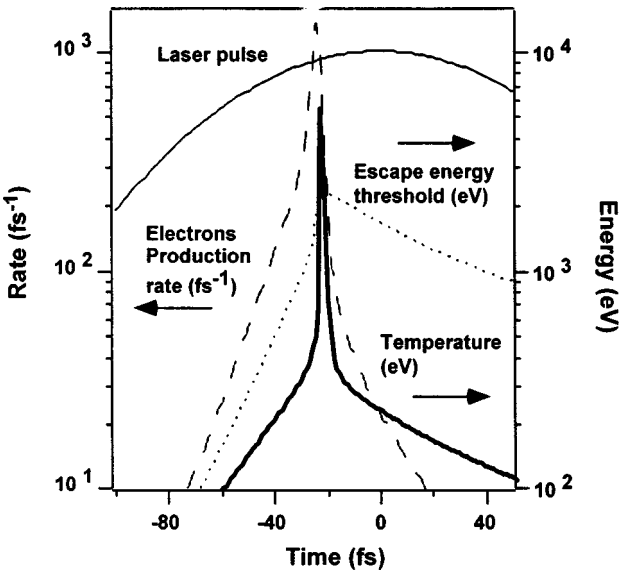

FIG. 16. Time history of 25-Å Xe cluster (1100 atoms/cluster) irradiated with a peak intensity of 1×10^{16} W cm^{-2} showing the laser pulse envelope (thin solid line), the electron temperature (thick solid line), the rate at which electrons exit the cluster by free streaming (dashed line), and the escape energy threshold (dotted line).

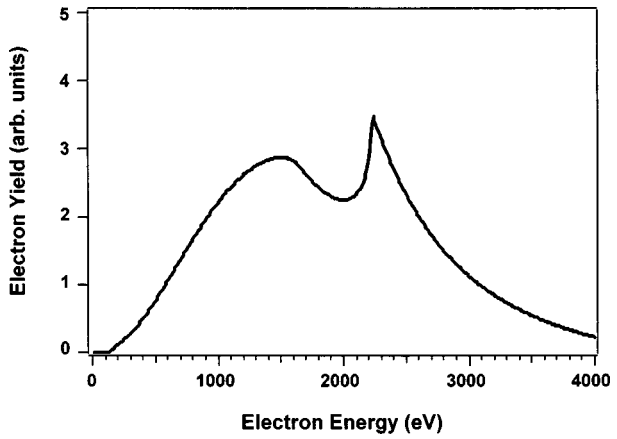

FIG. 17. Calculated electron energy spectrum for 25-Å Xe clusters (1100 atoms/cluster) irradiated by a 140-fs pulse with a peak intensity of 2×10^{16} W cm^{-2}.

Using these calculations it is possible to track the dynamics of the electrons escaping from the cluster during the process described in Fig. 15. Figure 16 shows the time history of a 25-Å Xe cluster ($\sim$1100 atoms) irradiated by a pulse with a peak intensity of 1×10^{16} W cm^{-2}. Here the electron temperature, laser pulse envelope, and escape energy threshold are shown, along with the calculated rate at which electrons exit the cluster by free streaming. As this figure illustrates, some electrons escape from the cluster in the initial stages of the cluster interaction as the electron temperature rises. However, once the electron temperature peaks due to the heating by the giant resonance, the electron escape rate also sharply peaks, since many of the electrons acquire enough thermal energy to overcome the space-charge forces of the cluster. This history implies that the electron energy spectrum might exhibit two features: one arising from the lower-energy electrons that escape from the cluster early in the interaction, and one from the hot electrons that escape during the resonance heating of the cluster.

The calculated electron distribution for the dynamics described in Fig. 16 is shown in Fig. 17. The distribution is found by summing the energy distribution of the electrons that leave the expanding cluster during the entire laser pulse. The calculated distribution does, in fact, exhibit a two-lobed distribution. Furthermore, it exhibits a close similarity to the measured electron distribution. The sharp peak near 2.5 keV is clearly consistent with the observed data, both in position and its narrow width. The calculation indicates that this peak in the data is evidence for the giant resonance in the heating of the electrons in the cluster spherical microplasma.

These calculations seem to explain the prominent features of the observed electron energy distribution. The model calculations indicate that the warm electron peak is the result of collisional heating of electrons near the surface of the cluster on the rising edge of the laser pulse. The hot electrons result from rapid heating of the remaining electrons in the bulk of the cluster later in the pulse when the electron density drops to a point to bring the heating into resonance. This explanation seems to be corroborated by the observed angular distribution data. The warm electrons are the result of some collisional heating early in the pulse. These electrons have undergone a limited number of collisions, broadening the angular distribution from that of purely tunnel-ionized electrons. The hot electrons, on the other hand, result from extensive collisional heating of the electrons in the bulk of the cluster. Consequently, their velocity distribution has been completely randomized, accounting for the isotropic distribution observed.

Though the calculated energy distribution exhibits close agreement with the measured distribution in the positions of the distribution peaks, the calculation does differ from the measured energy spectrum in some features. For example, the calculated distribution exhibits a hot electron peak with a broad tail. This is due to the assumption that the electron distribution within the cluster is a Maxwellian. In reality, the distribution within the cluster will not completely thermalize; the hottest electrons in the outer tail of the distribution leave the cluster first. The fast disassembly of the cluster prevents complete thermalization by electron-electron collisions, and there is insufficient time to populate the Maxwellian tail.

The production of hot electrons through inverse bremsstrahlung seen in the data and the calculation can drive a very energetic explosion of the cluster. This explosion is manifested in the very high energy ions observed. Charge separation of the hot electrons will inevitably drive a rapid expansion of the cluster. The explosion of the cluster can be driven by two forces. The first is the Coulomb repulsion between the highly charged ions in the cluster. If all the free electrons are retained in the cluster, the cluster is quasineutral and this force is negligible. However, the free streaming of electrons from the cluster will cause a charge buildup on the plasma sphere, and a Coulomb ''pressure'' will develop. We can make a simple estimate for the Coulomb pressure by assuming the cluster plasma is a good conductor and that any charge buildup on the sphere will reside on the surface. This assumption implies that the Coulomb pressure is [16]

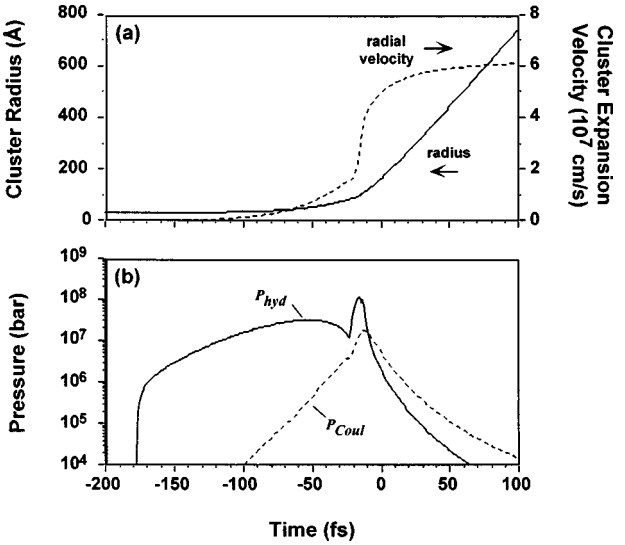

FIG. 18. (a) Time history of cluster radius and radial expansion velocity of a 32.5-Å Xe cluster (2300 atoms/cluster) irradiated by a 150 fs, 780-nm pulse at 2×10^{16} W cm^{-2}. (b) Hydrodynamic pressure and Coulomb pressure of the same cluster explosion.

$$P_{\mathrm{Coul}}=\frac{Q^2e^2}{8\pi R_c^4}, \tag{9}$$

where Qe is the charge residing on a cluster of radius R_c.

The second force important in driving the cluster explosion is the hydrodynamic pressure of the free electrons in the cluster. This force is present even if the cluster plasma remains neutral. The hot electrons in a plasma will set up a radial ambipolar potential that then accelerates the cluster ions. The pressure driving this expansion mechanism is simply

$$P_{\mathrm{hyd}}=n_ek_BT_e, \tag{10}$$

where T_e is the electron temperature. This hydrodynamic pressure is the same force that drives the expansion of a solid target plasma into vacuum after it has been heated by an intense laser pulse. In the interaction of picosecond pulses at intensities of $>10^{16}$ W cm^{-2} fast ions resulting from these plasmas have been observed with energies up to a few hundred keV [44].

The Coulomb explosion mechanism is similar to the mechanism that drives the explosion of small, optically ionized molecules. However, in bulk solid plasmas, the plasma remains quasineutral and the expansion is driven by the hydrodynamic force. This difference points to the question of which mechanism is responsible for the explosion of the clusters observed in our experiments. The Coulomb explosion force scales as $1/R_c^4$ while the hydrodynamic force scales as $1/R_c^3$. This suggests that Coulomb explosion forces may dominate for small clusters.

To investigate this physics, we can examine the relative contributions of the two forces on the expansion of a cluster in our uniform cluster plasma expansion model. The results of one such calculation are shown in Fig. 18 in which a 32.5-Å Xe cluster is irradiated by a 150-fs, 780-nm pulse with a peak intensity of 2×10^{16} W cm^{-2}. In Fig. 18(a) the temporal evolution of the cluster radius and radial velocity are shown. The cluster very rapidly expands during the pulse once heating of the electrons in the cluster has begun. The maximum radial ion energy is 255 keV, consistent with the very high ion energies observed in our experiment. The relative contributions of the hydrodynamic pressure and the Coulomb pressure are shown in Fig. 18(b). During the majority of the ion acceleration seen in Fig. 18(a), the dominant force is the hydrodynamic force, with very little contribution from the Coulomb explosion force. This analysis implies that the expansion of the exploding clusters is similar to that of an expanding plasma. Even for clusters of $\sim$1000 atoms the molecular picture of the explosion is no longer valid. It is also interesting to note that that electron pressure inside the cluster is very high. This calculation indicates that the electron pressure can exceed 100 Mbar for short period of time.

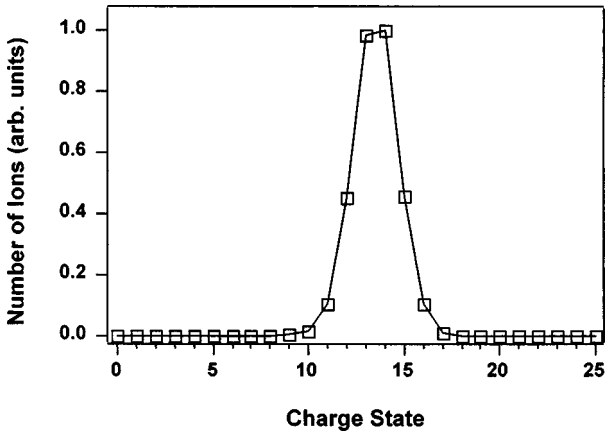

FIG. 19. Calculated charge-state distribution from a 32.5-Å Xe cluster (2300 atoms/cluster) irradiated by a 150-fs, 780-nm pulse at 2×10^{16} W cm^{-2}.

In light of the calculation of Fig. 18, the reasons for the very high energy ions observed can be very simply explained by a simple model. In the hydrodynamic expansion of the cluster both electrons and ions ultimately reach a velocity given roughly by the sound speed of the cluster plasma, $c_s=\sqrt{ZkT_e/m_i}$ (where kT_e is the electron thermal energy and m_i is the ion mass). Most of the resulting kinetic energy is, however, contained in the ions due to their much greater mass. On the basis of this statement, we expect that the average ion energy will be of the order of $\frac{1}{2}m_ic_s^2\sim ZkT_e$. This implies, for example, that the average Xe ion energy will be $\sim$50 keV if we assume that the electron temperature is given by the high-energy electron feature in Fig. 15(d), i.e., $kT_e\sim2.5$ keV and the average charge state is $Z\sim20^+$. This is in good agreement with our observed average Xe ion energies.

Our calculation also predicts the appearance of the high ion charge states observed ($>20^+$ for Xe ions). We find that rapid collisional ionization by the hot electrons within the cluster can strip the ions to very high charge states (up to Xe^{40+} in our calculations), a mechanism discussed at length in Ref. [16]. The calculated charge state of the Xe cluster calculation of Fig. 18 is shown in Fig. 19 after the cluster has expanded to infinity. This calculation implies that the Xe ions may become highly stripped. This calculation does not exactly match the measurement of Fig. 13, however, indicating that the ionization process in the cluster may be more complicated than the simple calculation.

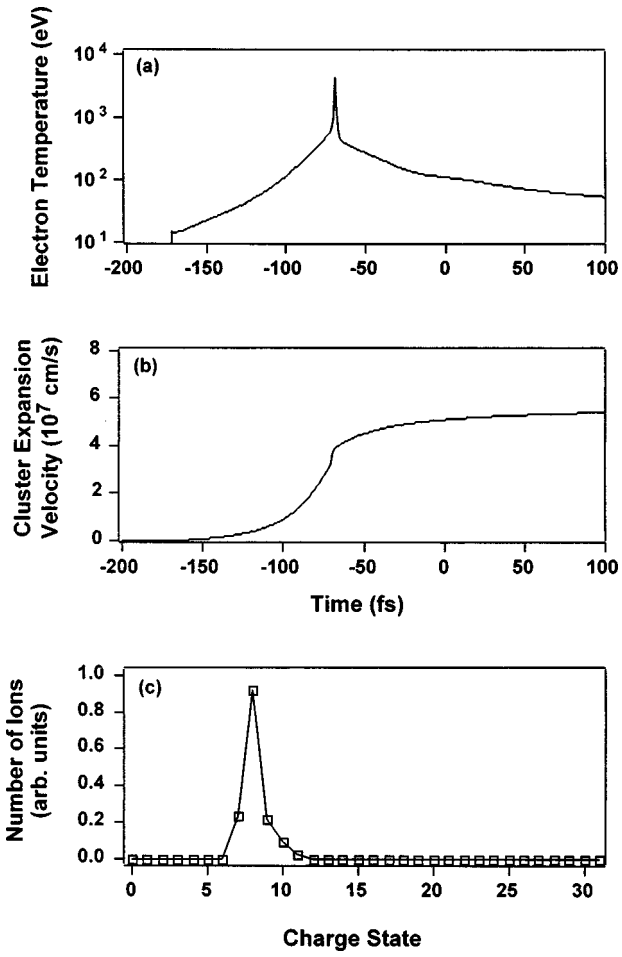

FIG. 20. (a) Calculated electron temperature and (b) cluster expansion velocity of a 2000-atom krypton cluster. (c) Charge-state distribution resulting from the cluster explosion.

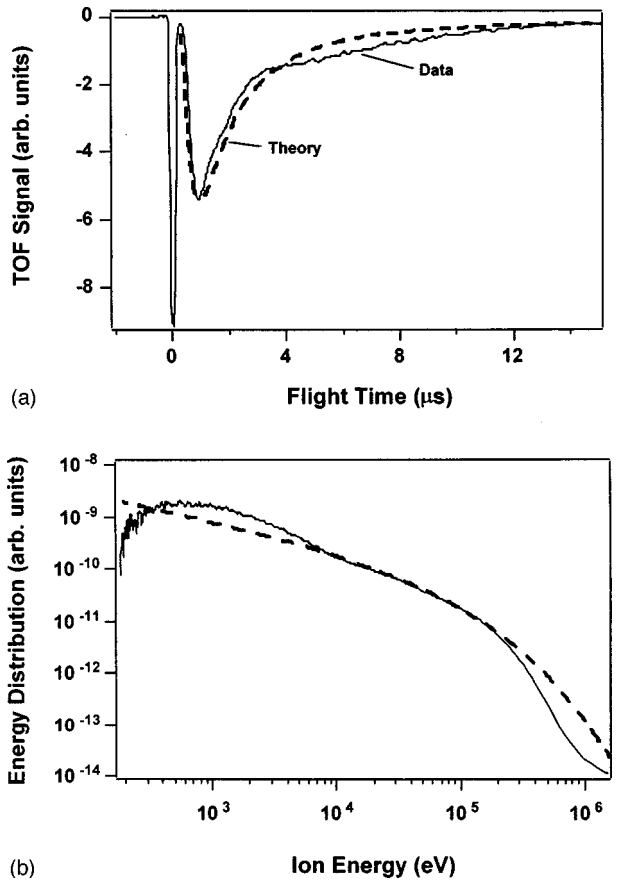

FIG. 21. Self-similar solution of ion energies resulting from the isothermal expansion of a Xe plasma with $Z=20$ and $T_e=2.5$ keV. Comparison of (a) calculated TOF trace and (b) ion energy spectrum with data.

We have also performed calculations for Kr clusters of similar size under our experimental conditions. We find that, in general, the dynamics are very similar to those of the exploding Xe clusters, with hydrodynamic forces dominant in driving the explosion, though the ion energies tend to be lower than those produced from the Xe clusters (~ 150 keV from 2000-atom Kr clusters). A calculation for a Kr cluster of 2000 atoms irradiated by a pulse with an intensity of 2×10^{16} W/cm^2 is shown in Fig. 20. The dynamics are very similar to the Xe clusters, but the resulting ion energies are lower. This is a result of the fact that the Kr ions are not as highly stripped as the Xe ions. This trend is confirmed by our experimental results, which also indicate that the Kr ions are not as highly charged as the Xe ions and that the Kr ions do not exhibit energies that are as high as those of the Xe ions under similar conditions.

Though the uniform plasma sphere model provides many insights into the cluster explosion dynamics and permits easy numerical calculations using a variety of physical effects, it is inadequate in predicting the shape of the ion distribution of an expanding plasma sphere. An experimental test of the hypothesis that the cluster expands primarily by hydrodynamic forces would be to compare the observed ion energy spectra with spectra calculated from the plasma fluid equations. Though including all the physics of the laser cluster interaction as discussed above is a prohibitively difficult numerical problem, it is possible to make some very good estimates of the resulting ion energy distribution for an expanding plasma by solving the plasma fluid equations alone, choosing suitable initial conditions to model the cluster.

If the cluster plasma is approximated by the classic two-fluid plasma model we can ignore the electron inertia compared to the more massive ion inertia and we retrieve the ion fluid equations [34]:

$$\frac{\partial n_i}{\partial t}+\frac{\partial}{\partial \mathbf{x}}\cdot(n_i\mathbf{u}_i)=0, \tag{11a}$$

$$\frac{\partial \mathbf{u}_i}{\partial t}+\left(\mathbf{u}_i\cdot\frac{\partial}{\partial \mathbf{x}}\right)\mathbf{u}_i=-\frac{Z}{n_e m_i}\frac{\partial p_e}{\partial \mathbf{x}}. \tag{11b}$$

Here n_i is the ion density, $\mathbf{u}_i$ is the ion velocity, Z is the charge state of the ions, m_i is the ion mass, and p_e is the electron pressure. The first equation is simply the conservation of mass equation, the second is the conservation of momentum. These equations describe the motion of an ion fluid subject to an electron pressure. The high-temperature electrons will set up an ambipolar potential that can accelerate the ions. This force is manifested in the right hand term of Eq. (11b).

To compare the predictions of these equations we must choose appropriate boundary conditions. We use the well-known self-similar solution of an isotropic, radial expansion

[34]. To calculate $dp_e/d\mathbf{x}$ we must choose an equation of state. For our simple estimate we use an isothermal equation of state. (Note that the actual expansion is not isothermal; the actual temperature is a complicated function of time. However, this calculation is intended only as a qualitative comparison and the temperature variation will not dramatically alter the shape of the calculated ion TOF trace.)

Figure 21(a) shows the self-similar solution of ion energies resulting from the isothermal expansion of an Xe plasma with $Z=20$ and an electron temperature of 2.5 keV (boundary conditions used because of the results of Figs. 4 and 13). This solution is compared with the measured ion TOF trace of Fig. 3. The measured TOF trace bears a striking similarity to that of the calculated hot-electron-driven hydrodynamic expansion. The resulting energy spectra are compared in Fig. (21b). The slope of the ion distribution is well reproduced by the calculation. The close similarity between the calculated hydrodynamic expansion and the observed ion energy distribution seems to confirm the assertion that the cluster explosion is largely driven by hydrodynamic forces.

V. CONCLUSION

In conclusion, we have studied the photoionization of noble-gas clusters by a high-intensity, femtosecond laser pulse. We have examined the energies of the electrons and ions produced in the explosion of the clusters and found that their kinetic energies are remarkably high. The electron energy distribution from the exploding clusters contains electrons with energies as high as 3 keV, which is several orders of magnitude higher than the energies observed in ATI of single atoms or small molecules. The ions produced in the explosion have mean energies of tens of keV and the maximum ion energy observed was 1 MeV. Ion charge states as high as Xe^{40+} have been observed.

These experimental observations are well explained by a theoretical model that treats the cluster as a small, spherical plasma. The cluster is ionized by optical and collisional ionization and begins to expand. The expansion of the cluster lowers the electron density to bring the electron oscillation into resonance with the electric field. This results in a very rapid deposition of energy into the electrons, causing a sharp spike in the electron temperature distribution. At this point, the ions are very rapidly stripped to high charge states by the hot electrons, and the cluster explodes. Collective phenomena, such as this resonant electron oscillation and heating, are very important in the interaction of light with clusters but are virtually absent in light-atom interactions.

The high ion energies and charge states observed in the explosion of clusters of a few hundred to a few thousand atoms in an intense laser field are very much like those observed in the expansion of a laser-heated solid-density plasma into vacuum. They contrast dramatically with the low-energy, low-charge-state ions produced in the Coulomb explosion of small molecules and clusters of only a few atoms in strong laser fields. Clusters of more than a few hundred atoms, therefore, represent an important transition in the dynamics of intense laser-matter interactions from molecules to solids.

[1] A. W. Castleman and R. G. Keesee, Science **241**, 36 (1988).

[2] B. Ernstberger, H. Krause, A. Kiermeier, and H. J. Neusser, J. Chem. Phys. **92**, 5285 (1990).

[3] S. Desai, C. S. Feigerle, and J. C. Miller, Z. Phys. D **26**, 220 (1993).

[4] S. Wei, W. B. Tzeng, and A. W. Castleman, J. Phys. Chem. **95**, 5080 (1991).

[5] Z. Y. Chen, C. D. Cogley, J. H. Hendricks, B. D. May, and A. W. Castleman, J. Chem. Phys. **93**, 3215 (1990).

[6] T. Nagata, J. Hirokawa, and T. Kondo, Chem. Phys. Lett. **176**, 526 (1991).

[7] J. T. Snodgrass, C. M. Roehl, and M. T. Bowers, Chem. Phys. Lett. **159**, 10 (1989).

[8] X. L. Li and R. L. Whetten, Chem. Phys. Lett. **196**, 535 (1992).

[9] C. Brechignac, P. Cahuzac, J. Leygnier, and A. Sarfati, Phys. Rev. Lett. **70**, 2036 (1993).

[10] J. Bregnacac and J. P. Connerade, J. Phys. B **27**, 3795 (1994).

[11] A. McPherson, T. S. Luk, B. D. Thompson, K. Boyer, and C. K. Rhodes, Appl. Phys. B: Photophys. Laser Chem. **57**, 337 (1993).

[12] A. McPherson, B. D. Thompson, A. B. Borisov, K. Boyer, and C. K. Rhodes, Nature (London) **370**, 631 (1994).

[13] A. McPherson, T. S. Luk, B. D. Thompson, A. B. Borisov, O. B. Shiryaev, X. Chen, K. Boyer, and C. K. Rhodes, Phys. Rev. Lett. **72**, 1810 (1994).

[14] J. Purnell, E. M. Snyder, S. Wei, and A. W. Castleman, Jr., Chem. Phys. Lett. **229**, 333 (1994).

[15] T. Ditmire, T. Donnelly, R. W. Falcone, and M. D. Perry, Phys. Rev. Lett. **75**, 3122 (1995).

[16] T. Ditmire, T. Donnelly, A. M. Rubenchik, R. W. Falcone, and M. D. Perry, Phys. Rev. A **53**, 3379 (1996).

[17] Y. L. Shao, T. Ditmire, J. W. G. Tisch, E. Springate, J. P. Marangos, and M. H. R. Hutchinson, Phys. Rev. Lett. **77**, 3343 (1996).

[18] T. Ditmire, J. W. G. Tisch, E. Springate, M. B. Mason, N. Hay, R. A. Smith, J. Marangos, and M. H. R. Hutchinson, Nature (London) **386**, 54 (1997).

[19] T. Ditmire, J. W. G. Tisch, E. Springate, M. B. Mason, H. Hay, J. P. Marangos, and M. H. R. Hutchinson, Phys. Rev. Lett. **78**, 2732 (1997).

[20] E. M. Snyder, S. Wei, J. Purnell, S. A. Buzza, and A. W. Castleman, Jr., Chem. Phys. Lett. **248**, 1 (1996).

[21] E. M. Snyder, S. A. Buzza, and A. W. Castleman, Phys. Rev. Lett. **77**, 3347 (1996).

[22] M. Lezius, S. Dobosz, D. Normand, and M. Schmidt, J. Phys. B **30**, L251 (1997).

[23] C. Rose-Petruck, K. J. Schafer, K. R. Wilson, and C. P. J. Barty, Phys. Rev. A **55**, 1182 (1997).

[24] A. L'Huillier, L. A. Lompre, G. Mainfray, and C. Manus, Phys. Rev. A **27**, 2503 (1983).

[25] S. Augst, D. D. Meyerhofer, D. Strickland, and S. L. Chin, J.

Opt. Soc. Am. B **8**, 858 (1991).
[26] U. Mohideen, M. H. Sher, H. W. K. Tom, G. D. Aumiller, O. R. Wood II, R. R. Freeman, J. Bokor, and P. H. Bucksbaum, Phys. Rev. Lett. **71**, 509 (1993).
[27] G. G. Paulus, W. Nicklich, H. Xu, P. Lambropoulos, and H. Walther, Phys. Rev. Lett. **72**, 2851 (1994).
[28] B. Walker, B. Sheehy, L. F. DiMauro, P. Agostini, K. J. Schafer, and K. C. Kulander, Phys. Rev. Lett. **73**, 1227 (1994).
[29] K. Codling and L. J. Frasinski, Contemp. Phys. **35**, 243 (1994).
[30] C. Cornaggia, M. Schmidt, and D. Normand, J. Phys. B **27**, L123 (1994).
[31] M. M. Murnane, H. C. Kapteyn, M. D. Rosen, and R. W. Falcone, Science **251**, 531 (1991).
[32] R. Shepherd, D. Price, W. White, S. Gordan, A. Osterheld, R. Walling, W. Goldstein, and R. Stewart, J. Quant. Spectrosc. Radiat. Transf. **51**, 357 (1994).
[33] S. J. Gitomer, R. D. Jones, F. Begay, A. W. Ehler, J. F. Kephart, and R. Kristal, Phys. Fluids **29**, 2679 (1986).
[34] L. M. Wickens and J. E. Allen, J. Plasma Phys. **22**, 167 (1979).
[35] C. Wülker, W. Theobald, D. Ouw, F. P. Schäfer, and B. N. Chichkov, Opt. Commun. **112**, 21 (1994).
[36] S. Hunsche, T. Starczewski, A. L'Huillier, A. Persson, C.-G. Wahlström, B. v. L. v. d. Heuvell, and S. Svanberg, Phys. Rev. Lett. **77**, 1966 (1996).
[37] D. J. Fraser and M. H. R. Hutchinson, J. Mod. Opt. **43**, 1055 (1996).
[38] O. F. Hagena and W. Obert, J. Chem. Phys. **56**, 1793 (1972).
[39] J. Wörmer, V. Guzielski, J. Stapelfeldt, and T. Möller, Chem. Phys. Lett. **159**, 321 (1989).
[40] M. V. Ammosov, N. B. Delone, and V. P. Krainov, Zh. Eksp. Teor. Fiz. **91**, 2008 (1986) [Sov. Phys. JETP **64**, 1191 (1986)].
[41] W. Lotz, Z. Phys. **216**, 241 (1968).
[42] V. P. Silin, Zh. Eksp. Teor. Fiz. **47**, 2256 (1964) [Sov. Phys. JETP **20**, 1510 (1965)].
[43] J. D. Jackson, *Classical Electrodynamics* (Wiley, New York, 1975).
[44] D. D. Meyerhofer, H. Chen, J. A. Delettrez, B. Soom, S. Uchida, and B. Yaakobi, Phys. Fluids B **5**, 2584 (1993).